ISSN 1392–1320 MATERIALS SCIENCE (MEDŽIAGOTYRA). Vol. 20, No. 4. 2014

A Geometry Information Based Fishnet Algorithm for Woven Fabric Draping in Liquid Composite Molding

Bo YANG [1], Tianguo JIN [1 *], Fengyang BI [1, 2], Jianguang LI [1]

[1] *School of Mechatronics Engineering, Harbin Institute of Technology, Harbin, 150001 China*
[2] *School of Mechatronics Engineering, Heilongjiang Institute of Technology, Harbin, 150001 China*

crossref http://dx.doi.org/10.5755/j01.ms.20.4.6075

Received 30 December 2013; accepted 27 April 2014

The draping of 2D textile fabrics is an important concern in the 3D composite parts manufacturing. The existing fitting algorithms for draping simulation are difficult to make a trade-off between flexibility, speed and accuracy. In the present work, a novel fishnet algorithm based on geometry information (GIB-fishnet algorithm) is proposed. Firstly, the fabric deformation modes during the draping process are analyzed, then several fundamental assumptions for draping simulation are proposed. Based on these assumptions and the theory of kinematic draping simulation, the GIB-fishnet algorithm is introduced, in this algorithm, geometry information of the surface such as tangent vector and normal curvature are used to determine the position of the current node. The use of the geometry information simplifies the mapping calculation and improves the computational accuracy. Two geometric algorithms for computing surface/surface intersection and seeking the shortest path on the surface, which are needed in the GIB-fishnet algorithm, are also studied in this paper. Finally, the simulation results of draping on three types of surfaces generated by different algorithms are compared, and the accuracy, speed and stability of the GIB-fishnet algorithm are verified.
Keywords: composite manufacturing; textile draping; geometry information; fishnet algorithm.

1. INTRODUCTION

Owing to their outstanding mechanical and structural properties, composite materials have been widely used in the aerospace industry. The design and manufacturing technologies of composite materials receive more and more attentions from researchers [1, 2]. While 3D weaving and braiding technologies used for direct manufacturing 3D composite parts are still immature and expensive, hence the 3D reinforcements are mainly obtained by draping of 2D textile fabrics [3, 4]. During the draping process, textile can adapt the complex 3D surface of the mold through yarn deformation and redistribution which bring great influence on the manufacturability and mechanical performance of the final composite products, so fabric draping study bears important theoretical and practical significance.

Computer simulation is an effective method for prediction of fabric draping, since it not only guides the draping operation, but also serves as a precondition of the simulation analysis of manufacturing processes and mechanical performance. Using the manufacturing process simulation of liquid composite molding (LCM) for a radome as an example, as shown in Fig. 1 [5]. The geometry model of the radome should be built firstly, then the draping simulation is conducted to obtain the yarn distribution parameters, such as local shear angle and local thickness and so on, based on those parameters, local permeability distribution can be computed, lastly, the filling process is simulated to evaluate the manufacturability of this radome. As can be seen from the example, the draping simulation of textile plays a function of connecting in the total manufacturing process analysis, it's a bridge of information exchange between design parameters (geometry model) and manufacturing analysis (mold-filling parameters prediction).

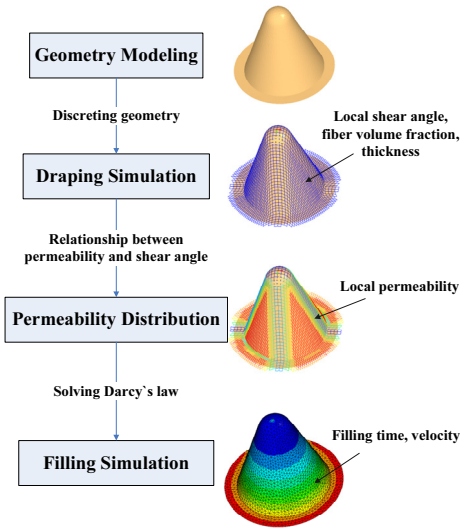

Fig. 1. Process of manufacturing simulation for a radome

Methods of draping simulation can be broadly grouped into two categories. First are the kinematic methods which essentially fit a flat fabric to the desired surface using mapping techniques [6 – 16]. This group wins the wide attention because of their special advantages such as high stability and flexibility. The second group is based on Finite Element techniques. The textile fabric is modeled as continuous medium, FEM is used to simulate the deformation process during fabric draping, so the time histories of stress and strain of fabric can be predicted to optimize the draping method [17 – 20].

*Corresponding author. Tel.: +86-13603635938, fax: +86-045186416045.
E-mail address: *jintg@hit. edu.cn* (T. Jin)

Mack and Taylor [6] firstly discussed the draping simulation method, they defined several basic assumptions for the model of woven cloth, and then proposed an algorithm, named fishnet algorithm, for predicting the woven draping. Based on the fishnet algorithm, Robertson et al. [7, 8] adjusted those basic assumptions to improve the prediction accuracy for sphere and cone, and proved the convergence through grid refinement of the textile. Van Der Weeën [9] extended this algorithm to arbitrary curved surfaces, he assumed that the yarns are placed on the surface along geodesic curves, then used the shooting method to determine the geodesic edge. Aono et al. [10] analyzed the influence of boundary conditions on simulation results of fishnet algorithm, presented a new method for specifying the boundary conditions to reduce the computational complexity and avoid the uncalculated regions. Trochu et al. [11] used kriging technique to generate a differentiable parametric model for complex surface, in this model the fishnet algorithm could perform fairly well even with relatively coarse mesh. Wang et al. [12] analyzed yarn slippage which is neglected in fishnet algorithm.

Compared with the second group of methods, the kinematic methods are more easily implemented and have good stability. However, the demands of accuracy and speed of the algorithm have not been satisfied very well. The basic fishnet algorithm considers yarn path between two adjacent nodes as straight line which causes a low accuracy to draping simulation of the curved surface. The geodesic fishnet algorithm determines the position of the current node by a series of geodesic line seeking calculations which are analytically intractable and time consuming, so it is rarely applied to simulate the draping of complex surfaces. The mosaic algorithm is a simplified version of fishnet algorithm which is based on a representation of the surface by an assembly of flat triangles, so the accuracy of the mosaic algorithm mainly depends on the discrete degree of the surface, a larger number of elements are needed for accurate approximation of the surface curvature, while the speed of calculating will slow down. In an effort to improve the efficiency and precision of the draping simulation, a novel fishnet algorithm based on the geometry information (GIB-fishnet algorithm) is presented in the current paper. GIB-fishnet algorithm transforms the node position determination problem into a series of surface/surface intersection problems with the use of geometry information such as normal vector and curvature, so the influence of the surface presentation on the simulation accuracy is reduced and the intensive computation is avoided. Comparisons between the GIB-fishnet algorithm and the existing algorithms by simulations of draping on several types of doubly-curved surfaces are also conducted in this paper.

2. DEFORMATION MODES OF TEXTILE FABRIC

Essentially, drape is the deformation of 2D fabrics caused by gravity, drape pressure and friction for adaptation of the fabrics on the mold surface, the following deformation modes can occur for one single textile layer: shearing, straightening, wrinkling, stretching and slipping, as shown in Fig. 2.

Fabric shear occurs if the directions of applied tensile forces don't coincide with the orientations of the yarn axes. The yarn orientations change until the yarn axes coincide with the directions of applied forces, or until a fabric specific maximum shear angle (locking angle) is achieved. Locking angles observed from experiments for various glass fiber woven fabrics are in the range between 15° and 35°. In case of fiber locking, the fabric starts to wrinkle due to the local shear stresses. Yarn straightening under tensile load in general is the deformation mode to occur first, while this effect is negligible for most low-crimp textile architectures due to the high elastic modulus of fibers. Yarn slippage usually only occurs at sharp edges or corners of the mold surface. From the parametric study carried by Chen and Govindaraj [21], we can find that the draping behavior is mainly determined by shear deformation because of the fabric's high elastic modul-us and low shear modulus. In consideration of this, the following assumptions can be made for draping simulation: (i) No slippage occurs at a crossing when the fabric is deformed; (ii) The yarn is inextensible; (iii) Warp and weft yarns can rotate frictionless around the cross point; (iv) Diameter of yarn and thickness of fabric are both negligible. The draping simulation algorithms based on those assumptions are collectively named fishnet algorithm.

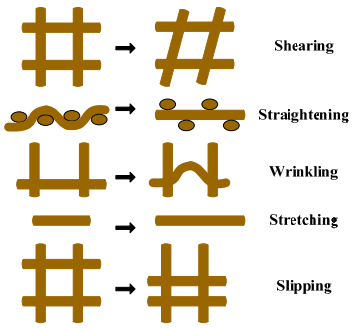

Fig. 2. Illustration of fabric deformation modes

3. THEORY OF KINEMATIC DRAPE SIMULATION

Each point $\boldsymbol{x}$ on the mold surface can be described parametrically in surface coordinates $u_i (i = 1, 2)$:

$$\boldsymbol{x} = \boldsymbol{x}(u_1, u_2), \tag{1}$$

where, $\boldsymbol{x} = (x_1, x_2, x_3)$.

Elementary arc lengths on the surface are given in the first fundamental form of the surface:

$$ds^2 = G_{ij} du_i du_j, i, j = 1,2, \tag{2}$$

where the coefficients

$$G_{ij} = \frac{\partial \boldsymbol{x}}{\partial u_i} \cdot \frac{\partial \boldsymbol{x}}{\partial u_j} = \frac{\partial x_1}{\partial u_i} \cdot \frac{\partial x_1}{\partial u_j} + \frac{\partial x_2}{\partial u_i} \cdot \frac{\partial x_2}{\partial u_j} + \frac{\partial x_3}{\partial u_i} \cdot \frac{\partial x_3}{\partial u_j}. \tag{3}$$

The two families of mutually orthogonal yarns of the fabric are described by coordinates v_i $(i = 1, 2)$ running in the yarn directions, and the elementary arc lengths on the deformed textile are given by

$$ds^2 = \left(\delta_{ij} + 2E_{ij}\right) dv_i dv_j, \tag{4}$$

where δ is Kroneker delta and E_{ij} are the components of the Green-Lagrange tensor, based on the assumptions (ii) and (iii), we have

$$\begin{cases} E_{11} = 0 \\ E_{22} = 0 \\ 2E_{12} = 2E_{21} = \cos\alpha \end{cases}, \quad (5)$$

where α is shear angle.

For deposition of the textile on the surface, equations (2) and (4) are equal:

$$G_{ij} du_i du_j = (\delta_{ij} + 2E_{ij}) dv_i dv_j . \quad (6)$$

Substitution of equations (3) and (5) in equation (6) gives

$$G_{11} du_1^2 + 2G_{12} du_1 du_2 + G_{22} du_2^2 = dv_1^2 + 2\cos\alpha dv_1 dv_2 + dv_2^2 . \quad (7)$$

So the drape of the fabric on the surface is described by mapping

$$\begin{cases} u_1 = u_1(v_1, v_2) \\ u_2 = u_2(v_1, v_2) \end{cases}. \quad (8)$$

Inserting of

$$\begin{aligned} du_1 &= \frac{\partial u_1}{\partial v_1} dv_1 + \frac{\partial u_1}{\partial v_2} dv_2 \\ du_2 &= \frac{\partial u_2}{\partial v_1} dv_1 + \frac{\partial u_2}{\partial v_2} dv_2 \end{aligned} \quad (9)$$

in equation (7) gives

$$\begin{aligned} &G_{11}\left(\frac{\partial u_1}{\partial v_1}\right)^2 + 2G_{12}\frac{\partial u_1}{\partial v_1}\frac{\partial u_2}{\partial v_1} + G_{22}\left(\frac{\partial u_2}{\partial v_1}\right)^2 = 1 \\ &G_{11}\left(\frac{\partial u_1}{\partial v_2}\right)^2 + 2G_{12}\frac{\partial u_1}{\partial v_2}\frac{\partial u_2}{\partial v_2} + G_{22}\left(\frac{\partial u_2}{\partial v_2}\right)^2 = 1 \\ &G_{11}\frac{\partial u_1}{\partial v_1}\frac{\partial u_1}{\partial v_2} + G_{12}\left(\frac{\partial u_1}{\partial v_1}\frac{\partial u_2}{\partial v_2} + \frac{\partial u_1}{\partial v_2}\frac{\partial u_2}{\partial v_1}\right) + G_{22}\frac{\partial u_2}{\partial v_1}\frac{\partial u_2}{\partial v_2} = \cos\alpha \end{aligned} \quad (10)$$

For solving equations (10), the initial fabric orientation, which is defined by a starting point on the surface and two curves along which the warp and weft will be fitted, should be preliminary determined. The two curves could be geodesics on the surface.

4. GEOMETRY INFORMATION BASED FISHNET ALGORITHM

A novel method for determining the positions of fabric nodes is described in this section, with this method, intensive computation needed for the existing draping algorithm is reduced, and the precision of the simulation is improved with the use of geometry information.

4.1. Mapping methodology

Mapping the flat fabric to the 3D surface is shown in Fig. 3. Suppose that the step distances of yarn in the weft and warp directions are both d, the undeformed fabric is shown in Fig. 3, a, and the fitted fabric on the mold surface after draping process is shown in Fig. 3, b.

At the start of mapping, the nodal coordinates of yarns $v_1 = 0$ and $v_2 = 0$ on the surface are already known, other nodes are determined one by one from the known nodal coordinates. For example, given the coordinates of nodes $(i, j-1)$ and $(i-1, j)$ as shown in Fig. 3, b, the coordinates of node (i, j) named "current node" can be generated based on the assumption (ii) described in section 2. The existing two algorithms for position determination of node (i, j) are respectively basic fishnet algorithm and geodesic algorithm. It is well known that a point on a surface has both position information and vector information, while the two algorithms mentioned above merely make use of the position information of nodes $(i, j-1)$ and $(i-1, j)$. Due to the characteristics of material and manufacturing process, the surfaces of composite parts have a shape of flat or small curvature, and the size of parts (m) is much larger than the fabric grid (mm), so the shear angles of neighboring grids on the fitted fabric are very close to each other, therefore the method described below can be used to determine the coordinates of the current node.

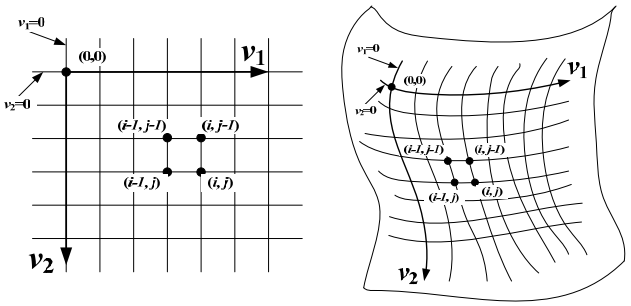

Fig. 3. Illustration of fabric mapping: a – undeformed fabric; b – mapping of the fabric to a surface

Determination of the position of the current node is shown in Fig. 4. The filled circles A, B and C indicate the known nodes $(i-1, j-1)$, $(i-1, j)$ and $(i, j-1)$. The solid line curve segments AB and AC indicate the yarn paths between node A and nodes B, C on the surface, the paths are also generated from the previous calculations, so the unit tangent vectors of both paths at point A, $\vec{r}_1$ and $\vec{r}_2$ shown in Fig. 4, can be obtained.

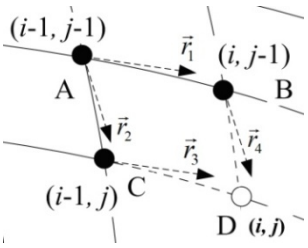

Fig. 4. Determination of current node

The hollow circle D shown in Fig. 4 indicates the current node (i, j), the hollowline curve segments CD and BD indicate yarn paths between node D and nodes B, C on the surface, the paths are still unknown. Supposing the unit tangent vectors of CD and BD at points C and B are $\vec{r}_3$, $\vec{r}_4$ as shown in Fig. 4, the following approximate equations can be proposed based on the previous analysis:

$$\vec{r}_3 \approx \vec{r}_1, \vec{r}_4 \approx \vec{r}_2 . \quad (11)$$

So $\vec{r}_1$ and $\vec{r}_2$ can be used as the approximate values of $\vec{r}_3$ and $\vec{r}_4$, then the normal curvatures of the surface at B and C in the directions $\vec{r}_3$ and $\vec{r}_4$ can be generated by

$$\kappa_n = S(\vec{r}) \cdot \vec{r} , \quad (12)$$

where S is the shape operator. Since the fabric grid is relatively small, the curvatures of the whole curve segment can be supposed as a constant value κ_n, then the curve segments CD and BD become two circular arcs with the radiuses of $1/\kappa_{nc}$ and $1/\kappa_{nb}$, so the node (i, j) synchronously

lies on two spherical surfaces expressed by equations (13) and (14):

$$\left(x_{i,j}-x_{i-1,j}\right)^2+\left(y_{i,j}-y_{i-1,j}\right)^2+\left(z_{i,j}-z_{i-1,j}\right)^2=l_c^2; \quad (13)$$

$$\left(x_{i,j}-x_{i,j-1}\right)^2+\left(y_{i,j}-y_{i,j-1}\right)^2+\left(z_{i,j}-z_{i,j-1}\right)^2=l_b^2, \quad (14)$$

where $l_x\,(x=b,c)$ indicate the straight-line distances between node (i,j) and nodes $(i,j-1)$, $(i-1,j)$, as shown in Fig. 5, which can be computed by

$$l_x=2\sin\frac{d\kappa_{nx}}{2}\Big/\kappa_{nx}, x=b,c. \quad (15)$$

After simultaneously solving equations (13), (14) and the equation of mold surface, the coordinates of node (i,j) can be determined, then the yarn paths CD and BD can be obtained by the geodesic line generation algorithm which will be described later in detail. Repeat the above process until the whole surface is covered.

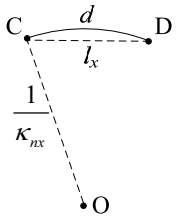

Fig. 5. Straight-line distance between D and B, C

In the above method, geometry information including both position information and vector information at the neighboring nodes is fully used for determining the current node position, so it is named geometry information based fishnet algorithm (GIB-Fishnet algorithm), its calculation flow is shown in Fig. 6.

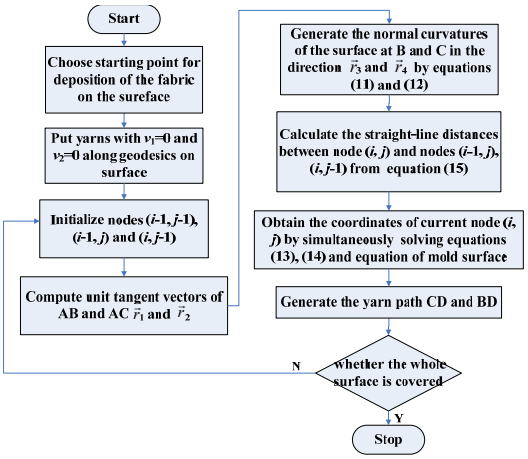

Fig. 6. Calculation flow of GIB-Fishnet algorithm

4.2. Surface/Surface intersection algorithm

Simultaneously solving the equations (13), (14) and the equation of mold surface is essentially a problem of finding the intersection points of three surfaces which are two spheres and the mold surface respectively. The two spherical surfaces are expressed by equations (13) and (14), the intersection of the two spheres is a circle which is placed on the plane:

$$Ex+Fy+Gz=H, \quad (16)$$

where

$$\begin{aligned}E&=2\left(x_{i,j-1}-x_{i-1,j}\right)\\F&=2\left(y_{i,j-1}-y_{i-1,j}\right)\\G&=2\left(z_{i,j-1}-z_{i-1,j}\right)\end{aligned}. \quad (17)$$

$$H=l_1^2-l_2^2+x_{i,j-1}^2-x_{i-1,j}^2+y_{i,j-1}^2-y_{i-1,j}^2+z_{i,j-1}^2-z_{i-1,j}^2$$

So the intersection circle can be expressed by

$$\begin{aligned}&\left(x-x_{i,j-1}\right)^2+(y-y_{i,j-1})^2+(z-z_{i,j-1})^2-l_2^2=\\&=Ex+Fy+Gz-H=0\end{aligned}. \quad (18)$$

Therefore, the problem of three surfaces intersection becomes a problem of curve/surface intersection problem. Supposing the mold surface is expressed by $m\times n$ degree NURBS surface:

$$\boldsymbol{r}(u,v)=\frac{\sum_{i=0}^{C_u-1}\sum_{j=0}^{C_v-1}w_{i,j}\boldsymbol{c}_{i,j}N_i^m(u)N_j^n(v)}{\sum_{i=0}^{C_u-1}\sum_{j=0}^{C_v-1}w_{i,j}N_i^m(u)N_j^n(v)}, \quad (19)$$

where the $\boldsymbol{c}_{i,j}$ are control points, the $w_{i,j}$ are weights, N is a B-spline basis function, C_u and C_v are the number of control points along the u and v axes, respectively.

Substituting equation (19) into equation (18), we obtain

$$\begin{cases}F_1(u,v)=\left(x(u,v)-x_B\right)^2+\left(y(u,v)-y_B\right)^2+\left(z(u,v)-z_B\right)^2-l_2^2=0\\F_2(u,v)=Ex(u,v)+Fy(u,v)+Gz(u,v)-H=0\end{cases}, \quad (20)$$

where $\boldsymbol{r}(u, v) = (x(u, v), y(u, v), z(u, v))$, F_1 and F_2 are both curve equations. The system of non-linear equations (20) can be solved by the Newton-Raphson method.

Assuming the first partial derivatives of the NURBS surface (19) with respect to variables u and v exist, let $(u^{(k)}, v^{(k)})$ denote the pair of variables at the k-th iteration, we can get the following relationship between $(k+1)$-th pair and the k-th pair:

$$\begin{bmatrix}u^{(k+1)}\\v^{(k+1)}\end{bmatrix}=\begin{bmatrix}u^{(k)}\\v^{(k)}\end{bmatrix}-\begin{bmatrix}\Delta u^{(k)}\\\Delta v^{(k)}\end{bmatrix}, \quad (21)$$

where

$$\begin{bmatrix}\frac{\partial F_1}{\partial u}&\frac{\partial F_1}{\partial v}\\\frac{\partial F_2}{\partial u}&\frac{\partial F_2}{\partial v}\end{bmatrix}\begin{bmatrix}\Delta u^{(k)}\\\Delta v^{(k)}\end{bmatrix}=\begin{bmatrix}F_1\left(u^{(k)},v^{(k)}\right)\\F_2\left(u^{(k)},v^{(k)}\right)\end{bmatrix}. \quad (22)$$

The initial condition defines the first approximated point at a position distance d_{uv} in uv space from the starting point in the direction $\boldsymbol{r}_a = (u_a, v_a)$ as follows:

$$\begin{bmatrix}u^{(0)}\\v^{(0)}\end{bmatrix}=\begin{bmatrix}u_0\\v_0\end{bmatrix}+d_{uv}\begin{bmatrix}u_a\\v_a\end{bmatrix}, \quad (23)$$

where

$$\boldsymbol{r}_a=u_a\frac{\partial \boldsymbol{r}}{\partial u}+v_a\frac{\partial \boldsymbol{r}}{\partial v}. \quad (24)$$

The distance d_{uv} is approximated by

$$d_{uv}=d_{xyz}R, \quad (25)$$

where R is the ratio of the length of a unit vector $\widetilde{\mathbf{V}}_{xyz}$ in xyz space to the length of the corresponding vector $\mathbf{V}_{uv}$ in uv space. $\widetilde{\mathbf{V}}_{xyz}$ is given as a parameter at the starting point. Once a new point is calculated, it is updated every time by

$$\widetilde{\mathbf{V}}_{xyz} = (\mathbf{P}_{-1} - \mathbf{P}_0)/\left|\mathbf{P}_{-1} - \mathbf{P}_0\right|, \tag{26}$$

where $\mathbf{P}_{-1} = (x_{-1}, y_{-1}, z_{-1})$ and $\mathbf{P}_0 = (x_0, y_0, z_0)$ indicate previous point and current point respectively. $\mathbf{V}_{uv}$ is obtained by the orthonormal projection of $\widetilde{\mathbf{V}}_{xyz}$ onto the tangent plane at $\mathbf{P}_0$.

The condition to finish iterative process is given as follows:

$$\left|F_1\left(u^{(k+1)}, v^{(k+1)}\right)\right| + \left|F_2\left(u^{(k+1)}, v^{(k+1)}\right)\right| < \varepsilon, \tag{27}$$

where ε is a small positive constant.

4.3. The shortest path between two points on a surface

After obtaining the position of the current node, the yarn paths on the mold surface between the neighboring nodes need to be determined. The generation of yarn paths CD and BD shown in Fig. 4 can be seen as a problem of seeking the shortest path between two points on a surface. Assuming the mold surface (19) is regular and non-periodic, Wolter [22] has proved the existence of the shortest path between two points on the surface, and the path is a geodesic line.

Let C be an arc length parameterized regular curve on surface (19) which passes through point P and is denoted by

$$\boldsymbol{r}(s) = \boldsymbol{r}(u(s)), v(s)). \tag{28}$$

Let $\boldsymbol{t}$ be a unit tangent vector of C at point P, $\boldsymbol{n}$ be a unit normal vector of C at point P, $\boldsymbol{N}$ be a unit normal vector of mold surface (19) and $\boldsymbol{w}$ be a unit vector perpendicular to $\boldsymbol{t}$ in the tangent plane defined by $\boldsymbol{N} \times \boldsymbol{t}$. The curvature vector $\boldsymbol{\kappa}$ of C into $\boldsymbol{w}$ component $\boldsymbol{\kappa}_g$ is called geodesic curvature vector, the geodesic curvature can be expressed by

$$\boldsymbol{\kappa}_g = (\boldsymbol{\kappa} \cdot \boldsymbol{w})\boldsymbol{w}, \tag{29}$$

which can be transformed to the following equation after deducing:

$$\kappa_g = \left[\Gamma_{11}^2\left(\frac{du}{ds}\right)^3 + \left(2\Gamma_{12}^2 - \Gamma_{11}^1\right)\left(\frac{du}{ds}\right)^2\frac{dv}{ds} + \left(\Gamma_{22}^2 - 2\Gamma_{12}^1\right)\frac{du}{ds}\left(\frac{dv}{ds}\right)^2 - \Gamma_{22}^1\left(\frac{dv}{ds}\right)^3 + \frac{du}{ds}\frac{d^2v}{ds^2} - \frac{d^2u}{ds^2}\frac{dv}{ds}\right]\sqrt{EG - F^2}, \tag{30}$$

where Γ_{ij}^i $(i, j, k = 1, 2)$ denote Christoffel symbols

$$\Gamma_{11}^1 = \frac{GE_u - 2FF_u + FE_v}{2(EG - F^2)} \quad \Gamma_{11}^2 = \frac{2EF_u - EE_v + FE_u}{2(EG - F^2)}$$
$$\Gamma_{12}^1 = \frac{GE_v - FG_u}{2(EG - F^2)} \quad \Gamma_{12}^2 = \frac{EG_u - FE_v}{2(EG - F^2)} \tag{31}$$
$$\Gamma_{22}^1 = \frac{2GF_v - GG_u + FG_v}{2(EG - F^2)} \quad \Gamma_{22}^2 = \frac{EG_v - 2FF_v + FG_u}{2(EG - F^2)}$$

where E, F, G are coefficients of the first fundamental form of the surface.

According to the definition of geodesic path, geodesics are curves of zero geodesic curvature. So the differential equation of geodesics can be described by

$$\kappa_g = 0, \tag{32}$$

Substituting equation (30) into equation (32), we obtain a system of second order ordinary differential equations which can be rewritten as a system of first order ordinary differential equations:

$$\frac{du}{ds} = p; \tag{33}$$

$$\frac{dv}{ds} = q; \tag{34}$$

$$\frac{dp}{ds} = -\Gamma_{11}^1 p^2 - 2\Gamma_{12}^1 pq - \Gamma_{22}^1 q^2; \tag{35}$$

$$\frac{dq}{ds} = -\Gamma_{11}^2 p^2 - 2\Gamma_{12}^2 pq - \Gamma_{22}^2 q^2. \tag{36}$$

Since the four boundary conditions for solving the system of four first order ordinary differential equations (33) to (36) are given at two points which are respectively the start (node B or C in Fig. 4) and the end (node D in Fig. 4) of the yarn segment, this is a boundary-value problem (BVP). General methods for the solutions of two-point BVPs can be found in [23, 24].

The system of differential equations (33)–(36) can be written in vector form for convenience. If we set

$$\begin{aligned}
&\boldsymbol{y} = (y_1, y_2, y_3, y_4)^T = (u, v, p, q)^T \\
&\boldsymbol{g} = (g_1, g_2, g_3, g_4)^T = (p, q, -\Gamma_{11}^1 p^2 - 2\Gamma_{12}^1 pq - \Gamma_{22}^1 q^2, \\
&-\Gamma_{11}^2 p^2 - 2\Gamma_{12}^2 pq - \Gamma_{22}^2 q^2)^T \\
&\boldsymbol{\alpha} = (\alpha_1, \alpha_2, \alpha_3, \alpha_4)^T, \boldsymbol{\beta} = (\beta_1, \beta_2, \beta_3, \beta_4)^T \\
&s \in [A, B]
\end{aligned}, \tag{37}$$

the equations (33)–(36) can be written as

$$\frac{d\boldsymbol{y}}{ds} = g(s, \boldsymbol{y}), \boldsymbol{y}(A) = \alpha, \boldsymbol{y}(B) = \beta. \tag{38}$$

A commonly used approach to the numerical solution of BVP is named relaxation method or finite difference method, this method starts with an initial guess and improves the solution iteratively.

Let us consider a mesh of points satisfying $A = s_1 < s_2 < \ldots < s_m = B$, then the four first order differential equations (38) can be approximated by the trapezoidal rule

$$\frac{\boldsymbol{Y}_k - \boldsymbol{Y}_{k-1}}{s_k - s_{k-1}} = \frac{1}{2}\left[\boldsymbol{G}_k + \boldsymbol{G}_{k-1}\right], k = 2,3,\ldots,m \tag{39}$$

with boundary conditions:

$$\boldsymbol{Y}_1 = \alpha, \boldsymbol{Y}_m = \beta, \tag{40}$$

where $\boldsymbol{Y}_k$ and $\boldsymbol{G}_k$ are the approximations of $\boldsymbol{y}(s_k)$ and $\boldsymbol{g}(s_k)$, $\boldsymbol{Y}_1$ and $\boldsymbol{Y}_m$ totally have 4 known components. Equation (39) forms a system of $4(m-1)$ nonlinear algebraic equations with $4m$ unknowns, the remaining 4 equations come from boundary conditions (40).

Let's refer to equation (39) as

$$\boldsymbol{F}_k = \left(F_{1,k}, F_{2,k}, F_{3,k}, F_{4,k}\right)^T = \frac{\boldsymbol{Y}_k - \boldsymbol{Y}_{k-1}}{s_k - s_{k-1}} - \frac{1}{2}\left[\boldsymbol{G}_k + \boldsymbol{G}_{k-1}\right] = 0, \tag{41}$$

$k = 2,3,\ldots,m$

where

$$\begin{aligned}
&F_{1,k} = u_k - u_{k-1} - \frac{1}{2}(s_k - s_{k-1})(p_k + p_{k-1}) = 0 \\
&F_{2,k} = v_k - v_{k-1} - \frac{1}{2}(s_k - s_{k-1})(q_k + q_{k-1}) = 0 \\
&F_{3,k} = p_k - p_{k-1} - \frac{1}{2}(s_k - s_{k-1})\left(\Gamma_{11,k}^1 p_k^2 + 2\Gamma_{12,k}^1 p_k q_k\right. \\
&\left. + \Gamma_{22,k}^1 q_k^2 + \Gamma_{11,k-1}^1 p_{k-1}^2 + 2\Gamma_{12,k-1}^1 p_{k-1} q_{k-1} + \Gamma_{22,k-1}^1 q_{k-1}^2\right) = 0 \\
&F_{4,k} = q_k - q_{k-1} - \frac{1}{2}(s_k - s_{k-1})\left(\Gamma_{11,k}^2 p_k^2 + 2\Gamma_{12,k}^2 p_k q_k\right. \\
&\left. + \Gamma_{22,k}^2 q_k^2 + \Gamma_{11,k-1}^1 p_{k-1}^2 + 2\Gamma_{12,k-1}^2 p_{k-1} q_{k-1} + \Gamma_{22,k-1}^2 q_{k-1}^2\right) = 0
\end{aligned} \tag{42}$$

and boundary conditions (40) as

$$\begin{aligned}\boldsymbol{F}_1 &= \left(F_{1,1}, F_{2,1}, ..., F_{n_1,1}\right)^T = \boldsymbol{Y}_1 - \alpha = 0 \\ \boldsymbol{F}_{m+1} &= \left(F_{1,m+1}, F_{2,m+1}, ..., F_{n_2,m+1}\right)^T = \boldsymbol{Y}_m - \beta = 0\end{aligned}, \tag{43}$$

here $n_1 + n_2 = 4$. Since we know the position of each boundary point on the geodesic segment, the parameters of equations (43) can be given by

$$\begin{aligned}F_{1,1} &= u_1 - u_A = 0 \\ F_{2,1} &= v_1 - v_A = 0 \\ F_{1,m+1} &= u_m - u_B = 0 \\ F_{2,m+1} &= v_m - v_B = 0\end{aligned}. \tag{44}$$

Then we have $4m$ equations:

$$\boldsymbol{F} = \left(F_1^T, F_2^T, ..., F_{m+1}^T\right)^T = 0 . \tag{45}$$

Equations (45) can be computed by quadratically convergent Newton iteration, if a sufficiently accurate starting vector $\boldsymbol{Y}^{(0)} = (\boldsymbol{Y}_1{}^T, \boldsymbol{Y}_2{}^T, ..., \boldsymbol{Y}_m{}^T)^T$ is provided. The Newton iteration scheme is given by

$$\boldsymbol{T}^{(i+1)} = \boldsymbol{Y}^{(i)} + \Delta\boldsymbol{Y}^{(i)}; \tag{46}$$

$$[\boldsymbol{J}^{(i)}]\Delta\boldsymbol{Y}^{(i)} = -\boldsymbol{F}^{(i)}, \tag{47}$$

where $[\boldsymbol{J}^{(i)}]$ is the $4m \times 4m$ Jacobian matrix of $\boldsymbol{F}^{(i)}$ with respect to $\boldsymbol{Y}^{(i)}$.

Since $\boldsymbol{F}_k$ are evaluated using information from points k and $k-1$, for non-boundary equations we only need to evaluate

$$\frac{\partial F_{i,k}}{\partial Y_{j,k-1}}, \frac{\partial F_{i,k}}{\partial Y_{j,k}} \quad i, j = 1,2,3,4 \quad k = 2,3....m \tag{48}$$

for boundary points, we evaluate

$$\frac{\partial F_{i,1}}{\partial Y_{j,1}}, \frac{\partial F_{i,m+1}}{\partial Y_{j,m}} \quad i = 1,2 \quad j = 1,2,3,4 . \tag{49}$$

Therefore the Jacobian matrix has the following block structure:

$$\begin{bmatrix} B_1 & & & & & & \\ A_2 & B_2 & & & & & \\ & A_3 & B_3 & & & & \\ & & A_4 & & & & \\ & & & . & & & \\ & & & & . & & \\ & & & & & B_{m-1} & \\ & & & & & A_m & B_m \\ & & & & & & A_{m+1} \end{bmatrix}, \tag{50}$$

where A_k B_k $(k = 2, 3, ..., m)$ are 4×4 submatrices obtained from equation (48), B_1 and A_{m+1} are 2×4 submatrices calculated from equation (49).

Substituting equations (45) and Jacobian matrix (50) into equation (47), we can get the correction vector $\Delta\boldsymbol{Y}$ as the following form:

$$\Delta\boldsymbol{Y} = \left(\Delta u_1, \Delta v_1, \Delta p_1, \Delta q_1, ..., \Delta u_m, \Delta v_m, \Delta p_m, \Delta q_m\right)^T . \tag{51}$$

To achieve more stability, our method employs a step correction procedure:

$$\boldsymbol{Y}^{(i+1)} = \boldsymbol{Y}^{(i)} + \mu\Delta\boldsymbol{Y}^{(i)}, \tag{52}$$

where $0 < \mu \le 1$ the value of μ should make the following equation hold:

$$\left\|\Delta\boldsymbol{Y}^{(i+1)}\right\|_1 < \left\|\Delta\boldsymbol{Y}^{(i)}\right\|_1 , \tag{53}$$

where $\|\Delta\boldsymbol{Y}\|_1$ is a scaled vector norm and defined as

$$\left\|\Delta\boldsymbol{Y}\right\|_1 = \sum_{k=1}^{m}\left(\frac{|\Delta u_k|}{M_u} + \frac{|\Delta v_k|}{M_v} + \frac{|\Delta p_k|}{M_p} + \frac{|\Delta q_k|}{M_q}\right), \tag{54}$$

here M_u, M_v, M_p, M_q are the scale factors for each variable in this work we set $M_u = M_v = 1$, $M_p = M_q = 10$. The iteration is terminated when the $\|\Delta\boldsymbol{Y}\|_1$ is small enough.

5. SIMULATION EXAMPLES AND DISCUSSION

5.1. Spherical surface

Since the analytical solution is available, the simulation of draping of textile fabric on a spherical surface is a benchmark for assessing the performance of the algorithm. Because of the symmetry, an octant of the sphere is used to be draped on, the simulation result obtained by GIB-fishnet algorithm is shown in Fig. 7, where the Boundary 1 and Boundary 2 indicate the boundary conditions $v_1 = 0$ and $v_2 = 0$.

From the geometric characteristics of the spherical surface, the analytic solution can be obtained conveniently [9], and the draping simulation was also conducted by different fishnet algorithms [9–11]. In Fig. 7, the dotted line connects the nodes with index $i = j$ on which the maximal shear angles of their spherical polar angles are achieved. The relationship between the maximal shear angle and spherical polar angle is shown in Fig. 8.

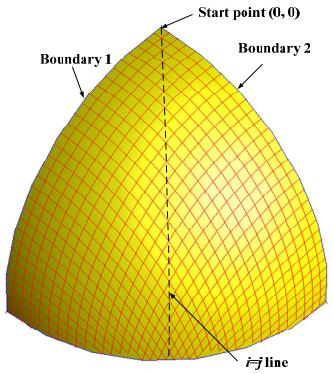

Fig. 7. Simulation result of draping on an octant of a sphere using GIB-fishnet algorithm

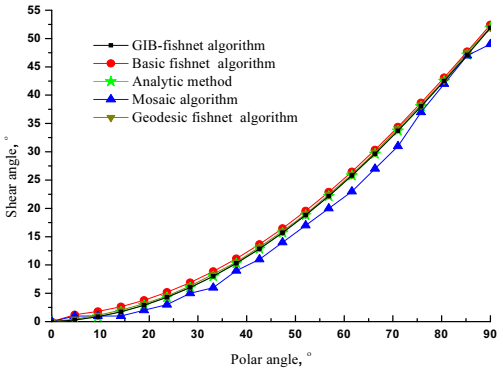

Fig. 8. Relationship between maximal shear and spherical polar angle

As can be seen from Fig. 8, mosaic algorithm has less accuracy. Compared to other algorithms, a larger

difference can be found between the simulation results of mosaic algorithm and analytic mdethod, and uncertain errors appear at different nodes. The reason is that mosaic algorithm disperses the surface with plane patches, the discrete forms and degrees of different regions depend on the surface local characteristics and discrete method, simulation of draping on the discrete surface will lead to an imprecise result with random errors, while the errors decrease with the reduction of the plane patch size. The basic fishnet algorithm considers the yarn segment between adjacent nodes as straight line, since the curvatures of spherical surface are equal everywhere, the errors of basic fishnet algorithm are equal on every node. Geodesic algorithm improves the simulation result of the basic algorithm, while it is impossible to achieve ideal value. On a spherical surface, since the normal curvatures of all nodes computed from equation (12) are equal, the GIB-fishnet algorithm generates the identical result as the analytical solution.

Fig. 9 shows the relationship between simulation time and grid size of textile, where the plane patch size for mosaic algorithm is 0.25*d*. GIB-fishnet algorithm has a higher computation speed than the geodesic algorithm, because it avoids the intensive computation during the geodesic seeking, while it is much slower than the other three algorithms because the geometric algorithms described in 4.2 and 4.3 are time-consuming.

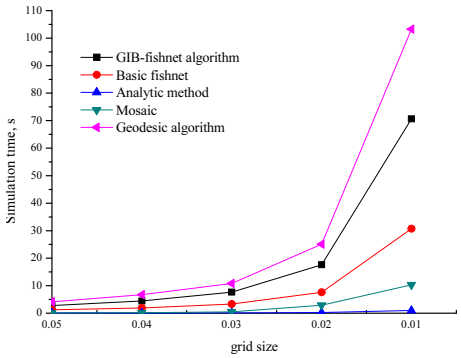

Fig. 9. Relationship between simulation time and grid size of woven

5.2. Saddle surface

Saddle surface is a kind of algebraic surface which can be expressed by

$$\frac{x^2}{2}-\frac{y^2}{2}-z=0\,. \tag{55}$$

Saddle surface is non-developable surface and it is difficult to obtain the analytical solution of the draping result. The simulation results of draping on the saddle surface using GIB-fishnet algorithm and a commercial draping simulation software, PAM-QUIKFORM, are shown in Fig. 10.

The whole saddle surface is divided into four parts by the boundaries as shown in Fig. 10, a, and the draping results are symmetric with each other. Take the lower right part as an example, nodes on $i=j$ dotted line attain the maximal shear angle of each yarn, and the other dotted line connects the nodes with index $i=20$. The relationships between shear angle and node position on the above mentioned dotted lines are shown in Fig. 11, including the two simulation results using GIB-fishnet algorithm and PAM-QUIKFORM (minus sign indicates the opposite shear direction).

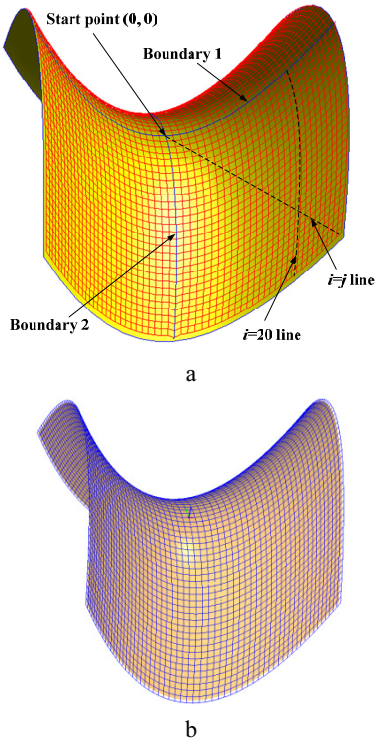

Fig. 10. Simulation results of draping on saddle surface: a – simulation result of GIB-fishnet algorithm; b – simulation result of PAM-QUIKFORM

Fig. 11 shows a good agreement between shear angles obtained by GIB-fishnet algorithm and PAM-QUIKFORM, it proves the feasibility and accuracy of the GIB-fishnet algorithm for draping simulation on algebraic surfaces. In addition, the maximal shear angles near the edge of surface are up to 50°, the data predicted from simulation can be used to guide the selection of reinforcing material and manufacturability evaluation for composite part.

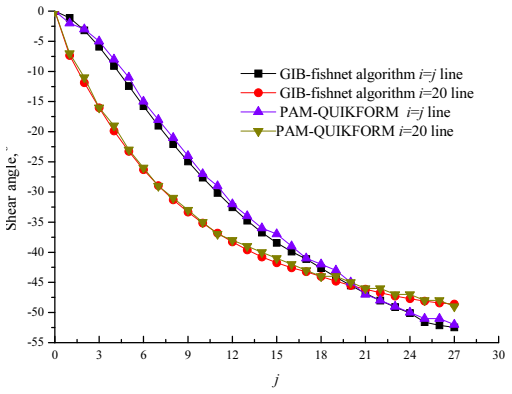

Fig. 11. Relationship between shear angle and node position

5.3. NURBS surface

A complex NURBS surface as shown in Fig. 12 is used to examine the GIB-fishnet algorithm. The surface is generated by specifying the control points, knot vectors and the associated weights, so it's impossible to get the analytical solution of draping on this surface. The

simulation results obtained by GIB-fishnet algorithm and PAM-QUIKFORM are also shown in Fig. 12, where the two dotted lines represent the similar node sequences as in Fig. 10, a, the relationships between shear angle and node position on the two dotted lines are shown in Fig. 13.

The shear angles of the simulation results coincide well with the expected values of PAM-QUIKFORM as can be seen from Fig. 13, the effectiveness of the GIB-fishnet algorithm for complex NURBS surface draping simulation is verified in this example.

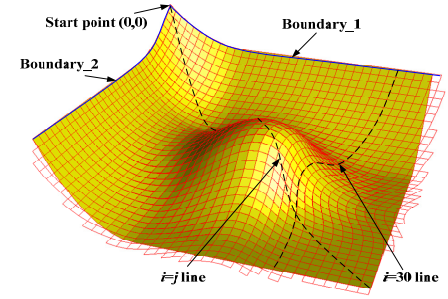

a

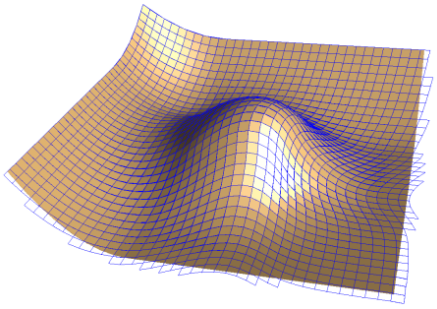

b

Fig. 12. Draping simulation result of a NURBS surface: a – simulation result of GIB-fishnet algorithm; b – simulation result of PAM-QUIKFORM

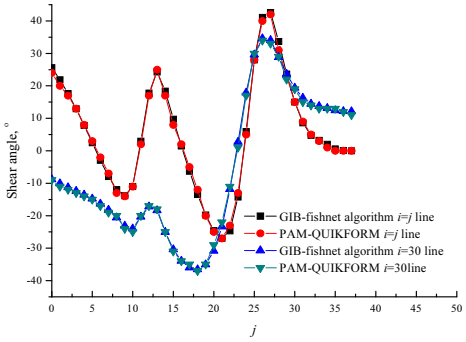

Fig. 13. Relationship between shear angle and node position

6. CONCLUSIONS

This paper presented a general technique for simulating the draping of 2D textile fabrics on 3D curved surfaces. Firstly, the deformation modes of fabric during the draping process were analyzed, a number of assumptions including the inextensibility of yarns were proposed. Then an overview of the theory of kinematic drape simulation was given.

A novel fishnet algorithm based on geometry information was proposed. As a key component of the fitting algorithm, a mapping methodology for determining the coordinates of the current node using the tangent vectors and curvatures of the nearby nodes on the surface was developed. This method provides greater rapidity and accuracy than the existing methods.

Two geometric methods for computing surface/surface intersection and seeking the shortest path of two points on a surface used in the GIB-fishnet algorithm are also studied, and in order to guarantee the universal applicability of the two methods, NURBS surface was used.

With three simulation experiments of a spherical surface, a saddle surface and a complex NURBS surface, the feasibility and accuracy of the GIB-fishnet algorithm were demonstrated. The results show that the GIB-fishnet algorithm has a higher accuracy and speed than the existing geodesic algorithm, and demonstrate that the GIB-fishnet algorithm is also effective for complex NURBS surface.

REFERENCES

1. **Arora, H.-S., Singh, H., Dhindaw, B.-K.** Composite Fabrication Using Friction Stir Processing – A Review *International Journal of Advanced Manufacturing Technology* 61 2012: pp. 1043 – 1055. http://dx.doi.org/10.1007/s00170-011-3758-8
2. **António, C.-A.-C., Davim, J.-P., Lapa, V.** Artificial Neural Network Based on Genetic Learning for Machining of Polyetheretherketone Composite Materials *International Journal of Advanced Manufacturing Technology* 39 2008: pp. 1101 – 1110.
3. **Mouritz, A.-P., Cox, B.-N.** A Mechanistic Interpretation of the Comparative In-plane Mechanical Properties of 3D Woven, Stitched and Pinned Composites *Composites Part A: Applied Science and Manufacturing* 41 2010: pp. 709 – 728. http://dx.doi.org/10.1016/j.compositesa.2010.02.001
4. **Glora, O.-A., Tariq, J., Ehsan, N., Mirza, E.** Strategy for Introducing 3D Fiber Reinforced Composites Weaving Technology *Procedia Technology* 1 2012: pp. 211 – 216.
5. **Mouton, S., Ledoux, Y., Teissandier, D., Sébastian, P.** Composite Part Design Based on Numerical Simulation of the Manufacturing Process *International Journal of Advanced Manufacturing Technology* 55 2011: pp. 421 – 431.
6. **Mack, C., Taylor, H.-M.** The Fitting of Woven Cloth to Surfaces *Journal of Textile Institute* 47 (8) 1956: pp. 477 – 488.
7. **Robertson, R.-E., Hsiue, E.-S., Sickafus, E.-N., Yeh, G.-S.-Y.** Fiber Rearrangements During the Molding of Continuous Fiber Composites. I: Flat Cloth to a Hemisphere *Polymer Composites* 2 (3) 1981: pp. 126 – 131. http://dx.doi.org/10.1002/pc.750020309
8. **Robertson, R.-E., Hsiue, E.-S., Yeh, G.-S.-Y.** Fiber Rearrangements During the Molding of Continuous Fiber Composites. II: Flat Cloth to a Rounded Cone *Polymer Composites* 5 (33) 1984: pp. 191 – 197.
9. **Van, D.-W.-F.** Algorithms for Draping Fabrics on Doubly-curved Surfaces *International Journal for Numerical Method in Engineering* 31 1991: pp. 1415 – 1426.
10. **Aono, M., Breen, D.-E., Wozny, M.-J.** Fitting a Woven-cloth Model to a Curved Surface: Mapping Algorithms *Computer-Aided Design* 26 (4) 1994: pp. 278 – 292. http://dx.doi.org/10.1016/0010-4485(94)90074-4

11. **Trochu, F., Hammami, A., Benoit, Y.** Prediction of Fiber Orientation and Net Shape Definition of Conplex Composite Parts *Composites Part A: Applied Science and Manufacturing* 27 A 1996: pp. 319 – 328.
12. **Wang, J., Paton, R., Page, J.-R.** The Draping of Woven Fabric Preforms and Prepregs for Production of Polymer Composite Components *Composites Part A: Applied Science and Manufacturing* 30 1999: pp. 757 – 765.
13. **Hancock, S.-G., Potter, K.-D.** The Use of Kinematic Drape Modelling to Inform the Hand Lay-up of Complex Composite Components Using Woven Reinforcements *Composites Part A: Applied Science and Manufacturing* 37 2006: pp. 413 – 422.
14. **Zhang, Y., Chen, L., Sun, F., Sun, Y., Li, Y., Tang, B., Liang, Z.** Experimental Research on Shear Deformation of Tackified Woven Fabrics *Acta Materiae Compositae Sinica* 26 (3) 2009: pp. 29 – 34.
15. **Chen, L., Zhang, Y., Sun, F., Sun, Y., Li, Y., Tang, B., Liang, Z.** Shear Model of Tackified Plain Fabrics *Acta Materiae Compositae Sinica* 27 (2) 2010: pp. 154 – 160.
16. **Zhang, Y., Jiang, Y., Qiu, G., Liu, L.** Formability of Multi-layered Biaxial Weft Knitted Fabrics on a Cylinder *Journal of Tianjin Polytechnic University* 24 (3) 2005: pp. 1 – 4.
17. **Pickett, A.-K., Creech, G., Luca, P.-D.** Simplified and Advanced Simulation Methods for Prediction of Fabric Draping *Reveu Europeenne des Elements* 14 2005: pp. 677 – 691.
18. **Boisse, P., Cherouat, A., Gelin, J.-C., Sabhi, H.** Experimental Study and Finite Element Simulation of a Glass Fiber Fabric Shaping Process *Polymer Composites* 16 (1) 1995: pp. 83 – 95.
19. **Sharma, S.-B., Sutcliffe, M.-P.-F.** A Simplified Finite Element Model for Draping of Woven Material *Composites Part A: Applied Science and Manufacturing* 35 2004: pp. 637 – 643. http://dx.doi.org/10.1016/j.compositesa.2004.02.013
20. **Skordos, A.-A., Monroy, A.-C., Sutcliffe, M.-P.-F.** A Simplified Rate Dependent Model of Forming and Wrinkling of Pre-impregnated Woven Composites *Composites Part A: Applied Science and Manufacturing* 38 2007: pp. 1318 – 1330. http://dx.doi.org/10.1016/j.compositesa.2006.11.005
21. **Chen, B., Govindaraj, M.** A Parametric Study of Fabric Drape *Textile Research Journal* 66 (1) 1996: pp. 17 – 24.
22. **Wolter, F.-E.** Interior Metric, Shortest Paths and Loops in Riemannian Manifolds with not Necessarily Smooth Boundary. Berlin, Germany: Free University of Berlin, 1979.
23. **Kimmel, R., Amir, A., Bruckstein, A.-M.** Finding Shortest Paths on Surfaces Using Level Sets Propagation *IEEE Transactions on Pattern Analysis and Machine Intelligence* 17 (6) 1995: pp. 635 – 640. http://dx.doi.org/10.1109/34.387512
24. **Takashi, M.** Computation of Shortest Paths on Free-form Parametric Surfaces *Journal of Mechanical Design, ASME Transactions* 118 (4) 1996: pp. 499 – 508. http://dx.doi.org/10.1115/1.2826919